iScience

CellPress
OPEN ACCESS

Article

Green synthesis of reduced graphene oxide by using tropical microalgae and its application in biophotovoltaic devices

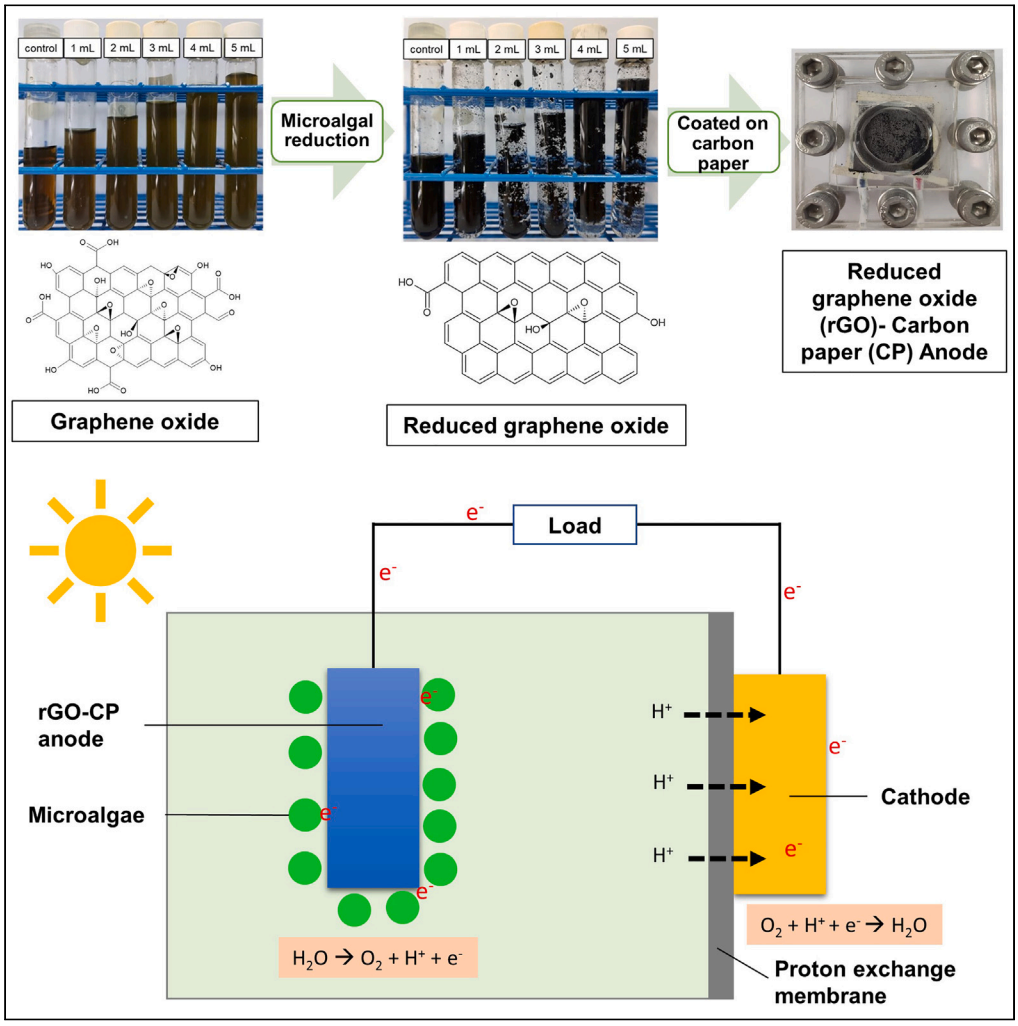

Jing-Ye Tee, Fong-Lee Ng, Fiona Seh-Lin Keng, ..., Shiwei Lin, G. Gnana kumar, Siew-Moi Phang

fonglee_ng@yahoo.com (F.-L.N.)
kumarg2006@gmail.com (G.G.k.)
phang@um.edu.my (S.-M.P.)

Highlights

The successful reduction of GO using *Chlorella* sp. UMACC 313 was achieved

The rGO was subsequently coated on the carbon paper and used as the anode of BPV

781% increase in maximum power density was achieved in rGO-CP compared to bare CP

rGO-CP BPV with *Synechococcus* sp. UMACC 371 achieved a power density of 0.555 mW m^{-2}

Tee et al., iScience *27*, 109564
April 19, 2024
https://doi.org/10.1016/j.isci.2024.109564

iScience

CellPress
OPEN ACCESS

Article

Green synthesis of reduced graphene oxide by using tropical microalgae and its application in biophotovoltaic devices

Jing-Ye Tee,[1,2] Fong-Lee Ng,[1,3,*] Fiona Seh-Lin Keng,[1,4] Choon-Weng Lee,[1,4] Bingqing Zhang,[5] Shiwei Lin,[5] G. Gnana kumar,[6,*] and Siew-Moi Phang[1,7,8,*]

SUMMARY

The successful commercialization of algal biophotovoltaics (BPV) technology hinges upon a multifaceted approach, encompassing factors such as the development of a cost-efficient and highly conductive anode material. To address this issue, we developed an environmentally benign method of producing reduced graphene oxide (rGO), using concentrated *Chlorella* sp. UMACC 313 suspensions as the reducing agent. The produced rGO was subsequently coated on the carbon paper (rGO-CP) and used as the BPV device's anode. As a result, maximum power density was increased by 950% for *Chlorella* sp. UMACC 258 (0.210 mW m^{-2}) and 781% for *Synechococcus* sp. UMACC 371 (0.555 mW m^{-2}) compared to bare CP. The improved microalgae adhesion to the anode and improved electrical conductivity of rGO brought on by the effective removal of oxygen functional groups may be the causes of this. This study has demonstrated how microalgal-reduced GO may improve the efficiency of algal BPV for producing bioelectricity.

INTRODUCTION

While fossil fuels currently dominate the world's primary energy output, their contribution to the greenhouse effect and the dwindling availability of fuel are spurring the search for diverse alternative energy solutions. The utilization of solar power is particularly appealing, given that the amount of light energy striking the Earth in 1 h is approximately equivalent to the world's annual energy consumption.[1] Microalgae, due to their growth rates, versatile product profiles, and ability to thrive under extreme environmental conditions, represent promising candidates for both harnessing solar energy and developing alternative energy sources.[2] Consequently, microalgae have undergone extensive study as feedstocks for various biofuels such as biodiesel, biohydrogen, and bioethanol.[3–5] Additionally, researchers have explored the utilization of microalgae in fuel cells, giving rise to a new variety of systems called biophotovoltaics (BPV). These systems not only generate bioelectricity but also provide unique facets including carbon sequestration, bioremediation, and biomass production.[6,7]

A hindrance in the commercialization of BPV is the suboptimal efficiency of extracellular electron transfer (EET) from the microalgae to the anode, resulting in reduced power generation.[8] Efforts have concentrated on enhancing anode attributes through surface treatment using catalysts or the development of novel anode materials.[9,10] Other than excellent electrical conductivity and durability, the anode should be biocompatible with microalgae, thereby promoting the cell adhesion and development of biofilm on the anode.[11] In this context, researches on the effect of different anode materials on the performance of BPV have been conducted, such as indium tin oxide (ITO),[12] fluorine-doped tin oxide (FTO)-coated ceramics,[13] and carbon nanotube (CNT)-modified carbon paper (CP).[14] Additionally, anode modifications with conductive materials or catalyst such as polypyrrole,[15] $FeWO_4/CeO_2$,[16] and metal organic frameworks[17] have been investigated. Nonetheless, their practical implementation is impeded by the intricate manufacturing processes, the expense of materials, and time-consuming procedures. Hence, a facile anode modification method employing cost-effective, electrochemically active, and durable materials is vital for the industrial viability of BPV technology.

Graphene, discovered in 2004, has garnered immense interest due to its remarkable physicochemical characteristics such as extensive surface area (2600 m^2/g), robust mechanical strength (Young's modulus of 10 TPA), and excellent electron mobility (15,000 $cm^2\ V^{-1}\ s^{-1}$).[18] However, due to its costly, low-yield, and complicated production methods, the commercialization of graphene has not yet been achieved. Among the production methods, the oxidation of graphite to graphene oxide (GO) followed by reduction to form reduced graphene oxide

[1]Institute of Ocean and Earth Sciences (IOES), Universiti Malaya, Kuala Lumpur 50603, Malaysia
[2]Institute for Advanced Studies, Universiti Malaya, Kuala Lumpur 50603, Malaysia
[3]School of Biosciences, Taylor's University, Lakeside Campus, Subang Jaya 47500, Selangor Darul Ehsan, Malaysia
[4]Institute of Biological Sciences, Faculty of Science, Universiti Malaya, Kuala Lumpur 50603, Malaysia
[5]State Key Laboratory of Marine Resource Utilization in South China Sea, School of Materials Science and Engineering, Hainan University, Haikou 570228, China
[6]Department of Physical Chemistry, School of Chemistry, Madurai Kamaraj University, Madurai 625021, Tamil Nadu, India
[7]Faculty of Applied Sciences, UCSI University, Jalan Puncak Menara Gading, Taman Connaught, Kuala Lumpur 56000, Malaysia
[8]Lead contact
*Correspondence: fonglee_ng@yahoo.com (F.-L.N.), kumarg2006@gmail.com (G.G.k.), phang@um.edu.my (S.-M.P.)
https://doi.org/10.1016/j.isci.2024.109564

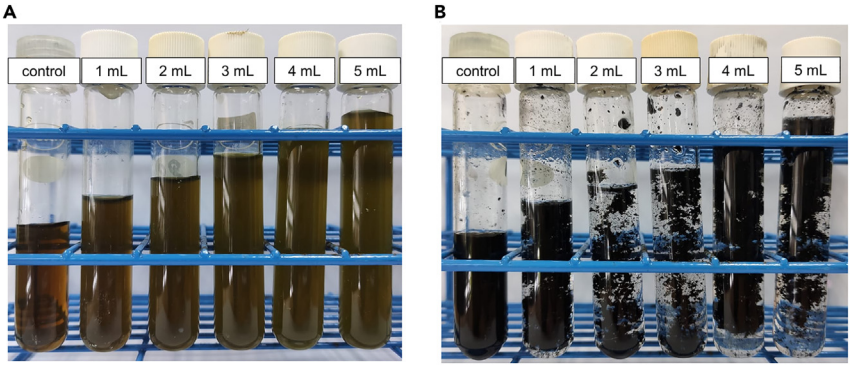

Figure 1. Photograph of GO before and after 72 h

(A) Photograph of GO before and (B) after 72 h with different volume of *Chlorella* sp. UMACC 313 suspensions (OD_{620nm}: 2.0).

(rGO) has emerged as a most promising approach in large-scale production of graphene.[19] GO contains oxygen functional groups such as hydroxyl, epoxy, carbonyl, and carboxyl groups which increase the hydrophilicity of GO, thus easy to be processed in solution in large quantities at low costs. Nonetheless, it disrupts the conjugated sp^2 network of the graphene sheets, thereby decreasing the electrical conductivity of GO. In order to restore the intrinsic properties of graphene, notably its electrical properties, the oxygen functional groups must be removed.[20]

Chemical reductants such as hydrazine hydrate, sodium borohydride, and hydroquinone have been used extensively to reduce GO. Yet, the utilization of chemical reductants has several limitations such as toxicity, potential doping, chemical selectivity, and waste production, which in turn results in high costs.[20] Thus, focus has shifted to biological reducing agents such as biomolecules,[21] plant extracts,[22] and bacteria.[23] However, obtaining large amount of these materials can be difficult as additional extraction processes are required which further increase the overall cost.[20] Today, algae are drawing increased attention for their pivotal role in green nanoparticles synthesis, leveraging their abundant availability and environmentally friendly characteristics. Algal cells contain a variety of bioactive compounds such as proteins, polysaccharides, pigments, and antioxidants, which has already been utilized as reductants to synthesize metal nanoparticles.[24,25] For instance, research has documented the successful synthesis of Ag and Au nanoplates through the reduction of metal ions using *Chlorella vulgaris*, with proteins emerging as primary biomolecules facilitating the reduction reaction.[26,27] Additionally, microalgae's ease of large-scale and cost-effective cultivation due to their rapid growth rate,[28] positions them as a promising environmental friendly option as a green reductant for producing rGO on a significant scale, employing a less energy intensive and non-toxic approach. rGO with its porous structure and substantial surface area, has been studied as an anode catalyst in microbial fuel cells (MFC) due to its excellent microorganism biocompatibility.[29,30] Studies have shown that the rGO anode promoted the adherence of microalgal cells onto the anode, thereby enhancing the EET efficiency from the microalgae to the anode.[31,32]

In line with this, we present our successful reduction of GO using *Chlorella* sp. UMACC 313 suspensions. Furthermore, we explored its application as the catalyst on the anode of algal BPV devices, aiming to enhance the efficiency of the device. This is the first study on the application of green synthesis of rGO-modified anode in algal BPV device, Moreover, the ability of tropical marine microalgae, *Chlorella* sp. UMACC 258 and *Synechococcus* sp. UMACC 371 in generating bioelectricity was evaluated.

RESULTS AND DISCUSSION

Reduction of graphene oxide

The successful reduction of GO by the *Chlorella* sp. UMACC 313 suspensions was indicated by the color change of the solution from yellowish-brown to black (Figures 1A and 1B).[33] The removal of oxygen-functional groups also caused the rGO to agglomerate and precipitate from the suspension, increasing its hydrophobicity and rendering it insoluble in water.[34]

The reduction of GO was also tracked using UV-vis spectroscopy (Figure 2A). The UV-vis spectrum of GO displays a maximum absorption peak (λ_{max}) at 230 nm, which is associated with the $\pi \rightarrow \pi^*$ transition of aromatic C–C bonds. A faint shoulder at approximately 300 nm, corresponding to the $n \rightarrow \pi^*$ transition of the C=O bonds, was also detected.[35,36] As GO underwent reduction by the *Chlorella* sp. UMACC 313 suspensions, the λ_{max} progressively shifted to 267 nm over a span of 72 h, signifying the restoration of the aromatic structure and electronic conjugation within rGO.[37] There were no additional alterations in the λ_{max} of rGO with extended reaction durations, aligning with the pattern seen in the reduction of GO using other environmentally friendly reducing agents like ascorbic acid,[21] root extract,[22] and *Escherichia coli*.[36]

Figure 2B illustrates the examination of the effect of *Chlorella* sp. UMACC 313 suspension volume on the reduction of GO. With statistical significance ($p < 0.05$), it was found that adding more than 3 mL of microalgal suspensions (OD_{620nm}: 2.0) did not result in a significant rise in λ_{max} even after 72 h. Accordingly, 3 mL of microalgal suspension is the optimum amount for efficiently reducing 5 mL of GO at a concentration of 0.5 mg mL^{-1}. A slight reduction of GO was observed from the control setup could be attributed to the application of heat during reduction in the 90°C water bath, which helps break the chemical bonds between the oxygen and carbon atoms in the GO.[20] Nevertheless, it should be

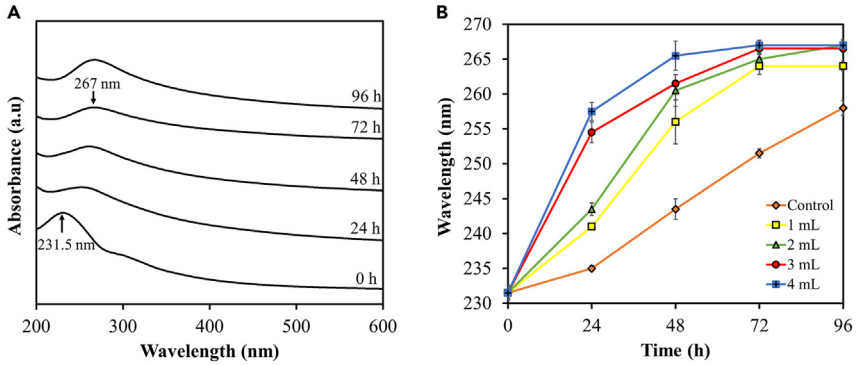

Figure 2. Investigation of the GO reduction process with *Chlorella* sp. UMACC 313 suspensions under varied reaction times and suspension volumes

(A) UV-vis absorption spectra of the rGO suspension at different reaction time; (B) Maximum absorbance peak of rGO suspension with different volume of *Chlorella* sp. UMACC 313 suspensions (OD_{620nm}: 2.0) across different reaction time. Data as mean ± S.D., (n = 4).

noted that the reduction degree of GO with *Chlorella* sp. UMACC 313 suspensions was significantly higher than the control setup, as observed from the UV-vis absorption spectra, which again shows that microalgal cells were the primary contributors to the reduction of GO.

Characterization of graphene oxide and reduced graphene oxide

The crystalline structures of GO and rGO were investigated by X-ray diffraction (XRD), as shown in Figure 3A. The *d*-spacing, defined as the distance between two graphene sheets, was calculated by using Bragg's equation, $n\lambda = 2 \text{ days } \sin\Theta$.[38] Typically, the XRD pattern of graphite exhibits a distinct basal reflection peak at $2\theta = 26.6°$, corresponding to a *d*-spacing of 0.335 nm. Conversely, GO establishes a prominent peak at 10.6° with a corresponding *d*-spacing of 0.84 nm. This observation suggests the intercalation of water molecules and oxygen functional groups between the layers of graphene sheets in GO.[35] After the reduction process, the distinctive peak associated with GO vanishes, and in its place, a broader peak emerges at approximately 22°. This indicates a *d*-spacing of 0.4 nm, which is quite close to, but notably larger than, the interlayer distance observed in pristine graphite.[39] This phenomenon could be ascribed to the partial elimination of oxygen functional groups.

The structural characterization of the prepared nanostructures was conducted using Fourier transform infrared spectroscopy (FT-IR) spectroscopy (Figure 3B). The FT-IR spectrum of GO shows a prominent peak at 3,196 cm^{-1}, attributed to the −OH stretching vibrations and the peak at 1,720 cm^{-1} corresponds to the C=O stretching vibration of carboxylic groups located at the edges of the GO sheets.[35] The peaks observed at 1,364, 1,218 and 1,043 cm^{-1} represent the C−O stretching vibrations, respectively, of carboxyl, epoxy, and alkoxy groups and the C=C stretching vibration are scrutinized at 1,618 cm^{-1}.[39] After the reduction of GO, the intensities of the C=O and C−O stretching vibrations are decreased, indicating a decrease in the presence of oxygen functional groups. The emergence of a new peak at 2,911 cm^{-1} can be linked to the stretching vibrations of C–H bonds.[40] Moreover, the peak at 1,561 cm^{-1} indicates the presence of aromatic C=C bonds,[39] implying the restoration of the sp^2 lattice characteristic of pristine graphene after reduction by the microalgal cells.[41] No modification and doping of biomolecules from the microalgal cells was observed as all the functional groups detected can be attributed to the rGO.

Raman spectroscopy is a non-destructive method used to investigate the structural properties of carbon materials.[42] Generally, Raman spectroscopy of graphitic materials is characterized by two main features: the G band (~1580 cm^{-1}), resulting from the first-order scattering of the phonons of sp^2 carbons with E_{2g} symmetry, and the D band (~1350 cm^{-1}), arising from the breathing mode vibration of κ-point phonons of A_{1g} symmetry. The D band only becomes active in the presence of structural defects.[43] The Raman spectrum of GO (Figure 4A) shows

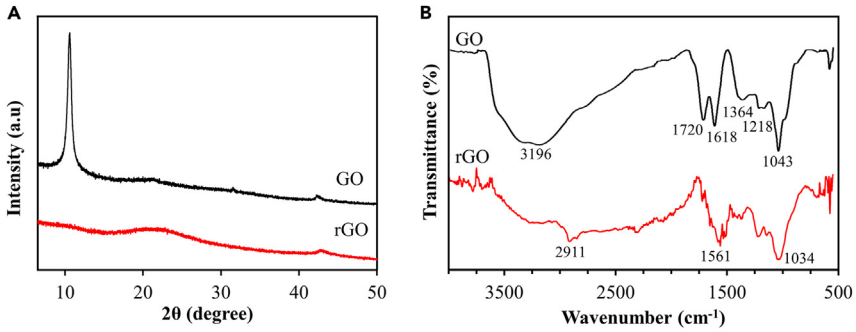

Figure 3. Characterization of GO and rGO using XRD and FTIR

(A) XRD patterns of GO and rGO; (B) FT-IR spectra of GO and rGO.

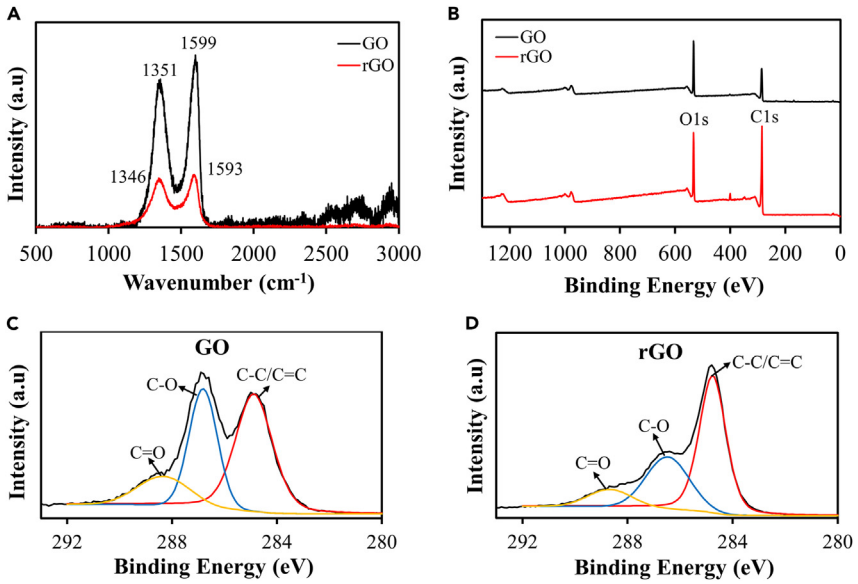

Figure 4. Characterization of GO and rGO using Raman and XPS

(A) Raman spectrum of GO and rGO; (B) XPS survey spectra of GO and rGO; C1s spectra of (C) GO and (D) rGO.

D and G bands, respectively, at 1,351 cm^{-1} and 1,599 cm^{-1} and scrutinized I_D/I_G ratio of 0.853. After the reduction process, the D and G bands of rGO shift, respectively, toward lower wavenumbers of 1,346 cm^{-1} and 1,593 cm^{-1}. Furthermore, the I_D/I_G ratio of rGO, which stands at 0.935 has risen in contrast to GO. This indicates a reduction in the average size of the sp^2 domains following the reduction process. This change may be attributed to the development of new, smaller sp^2 domains in rGO, which are more abundant than those found in GO prior to reduction.[34]

The X-ray photoelectron spectroscopy (XPS) was used to identify the atomic composition of the sample surface and the specific types of oxygen functional groups bonded to it.[44] The XPS survey spectra show the presence of carbon and oxygen elements in both GO and rGO samples. Notably, two prominent peaks observed at 284.8 eV and 532.6 eV correspond to C1s and O1s, respectively (Figure 4B). In the rGO sample, the intensity of C1s peak surpasses that in GO, implying the successful restoration of sp^2 carbon structure through reduction facilitated by the microalgal suspension.[45] The atomic carbon to oxygen (C/O) ratio of the GO and rGO was obtained by determining the ratio of C1s to O1s peak areas in the XPS survey spectra.[46] C/O ratio of rGO increased from 2.01 to 3.26, indicating the substantial removal of oxygen functional groups. This result is consistent with previous studies.[47,48] Figure 4C displays the C1s XPS spectrum of GO, revealing three distinct carbon bonding components: C–C/C=C (284.9 eV), C–O (286.8 eV), and C=O (288.4 eV).[34,46] In comparison to GO, the C1s spectrum of rGO shows noticeable reduction in the intensity of C–O and C=O peak, further suggesting the successful removal of oxygen functional groups from GO after reduction by the microalgal suspension (Figure 4D).[49]

Morphological properties

The surface morphology of GO-CP and rGO-CP was examined by using scanning electron microscope (SEM). SEM image of GO-CP displays a typical smooth and aggregated GO sheet coated on the CP (Figure 5A). Figure 5B shows the uneven distribution of smaller rGO flakes on the CP, which could be beneficial for the attachment of microalgal cells to the anode.[31,35] The reduction process led to the formation of smaller rGO flakes, consistent with the results from Raman analysis. The SEM images of *Chlorella* sp. UMACC 258 (Figure 5C) and *Synechococcus* sp. UMACC 371 (Figure 5D) biofilms grown on the rGO-CP show that rGO exhibits good biocompatibility with both marine microalgae species. This further confirms its suitability as an anode material for the algal BPV device.[50]

The microstructure of the as-synthesized rGO was further evaluated using transmission electron microscope (TEM) (Figure 6). TEM images confirm the formation of few-layered transparent rGO with a curved and wrinkled appearance, similar to previous report.[51] The darker areas indicate the stacking of several layers of rGO sheets, which could be due to van der Waals forces between the sheets upon the removal of oxygen functional groups.[52,53] Selected area electron diffraction (SAED) pattern of rGO (Figure 6C) shows a diffraction ring with some bright spots, indicating a lack of perfect crystallinity of the hexatomic ring due to the presence of defect after the reduction.[49]

Growth and photosynthetic efficiency of the marine microalgae

A typical growth curve based on chl-*a* of the two marine microalgae cultivated in the anodic chamber of BPV devices with an rGO-CP anode is shown in Figure 7A. The acquired growth curves show that rGO-CP is an appropriate material for the anode of BPV devices due to its biocompatibility with several species of microalgae.[31] *Chlorella* sp. UMACC 258 exhibits the specific growth rate of 0.038 $\pm$ 0.004 $days^{-1}$, while

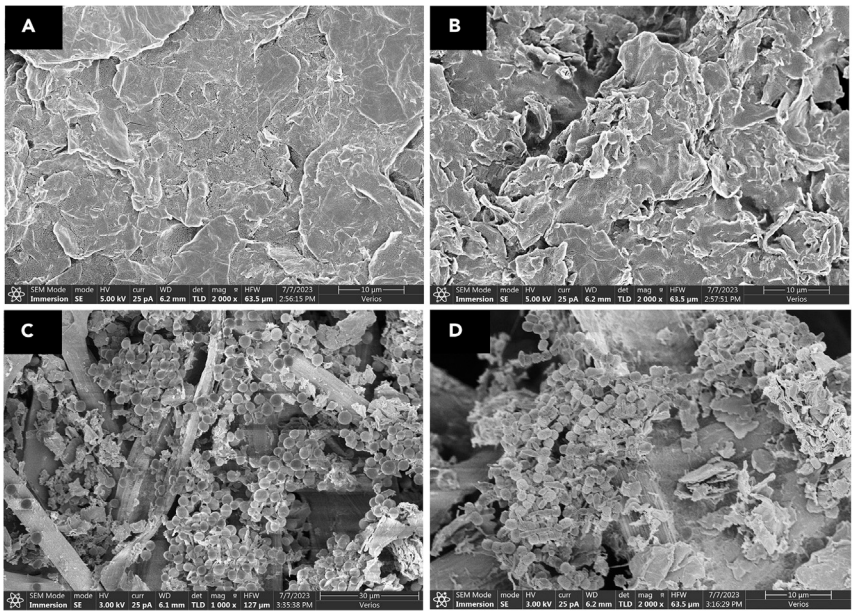

Figure 5. SEM image of GO and rGO

SEM image of (A) GO-CP (B) rGO-CP; (C) rGO-CP with *Chlorella* sp. UMACC 258 biofilms and (D) rGO-CP with *Synechoccocus* sp. UMACC 371 biofilm.

Synechococcus sp. UMACC 371 establishes the specific growth rate of 0.034 $\pm$ 0.007 days^{-1}. The physiological state of the marine microalgae was determined by measuring the maximum quantum yield (F_v/F_m) value (Figure 7B). For *Chlorella* sp. UMACC 258, this value varied from 0.35 to 0.60, while for *Synechococcus* sp. UMACC 371, it ranged from 0.14 to 0.37. It is crucial to highlight that F_v/F_m values ranging from 0.1 to 0.65 have been documented for microalgae in their natural environment. In general, the higher values typically indicate healthier cells, whereas lower values suggest opposite.[54] The declines in F_v/F_m values observed on day 8 and 12 could be due to the depletion of nutrients and the overpopulation of microalgal cells, aligning with the decrease in biomass.

Electrochemical analysis

The electrochemical activities of the as-synthesized anodes were evaluated using CV in *Chlorella* sp. UMACC 258 (Figure 8A) and *Synechococcus* sp. UMACC 371 (Figure 8B) cultures in Prov medium. The lowest current response observed for bare CP is due to the poor contact between the microalgae and the CP.[16] The biofilm-loaded CP exhibited higher current due to the improved contact between the microalgae and the CP, enhancing the EET.[17] Among the investigated anodes, the rGO-CP demonstrated the highest current. This can be attributed to the elimination of oxygen functional groups via the microalgal suspension, which enhanced the electrical conductivity of rGO.[35] Furthermore, the higher oxidation peak observed at 0.7 V vs. Ag/AgCl for the rGO-CP anode indicates the more efficient electron transfer from the electrochemically active membrane proteins located on the cellular surface of microalgae to the anode.[16] This could be due to the large surface area of rGO, improving the adhesion of microalgae to the anode and resulting in a better interaction between the microalgae and the rGO-CP anode.[31]

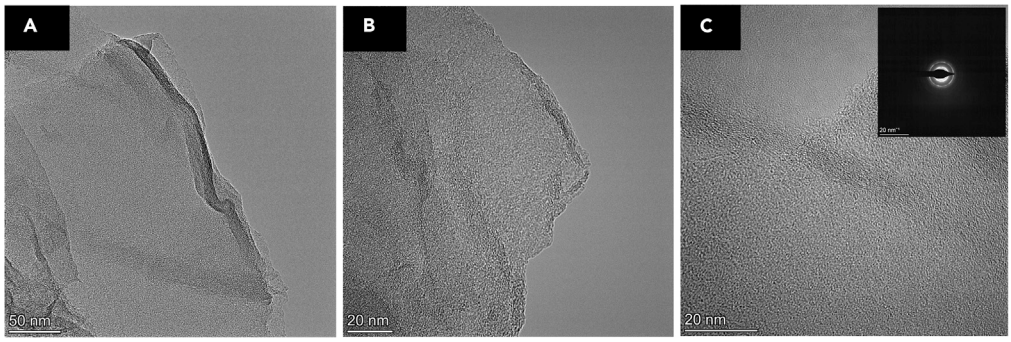

Figure 6. TEM image of rGO

(A–C) TEM image of rGO at different magnifications. Inset of (C): SAED pattern of rGO.

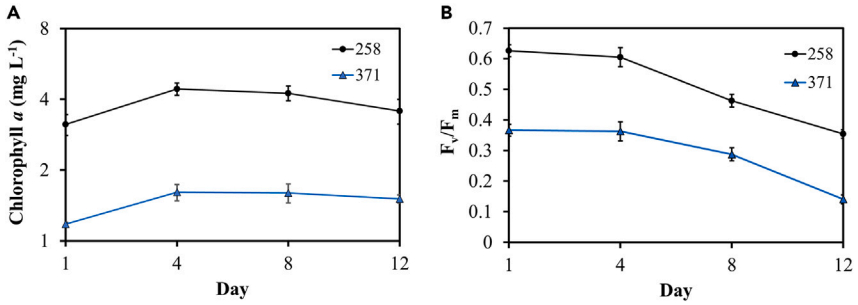

Figure 7. Growth and photosynthetic efficiency of the marine microalgae

(A) Growth curves based on chlorophyll *a* and (B) F_v/F_m values of *Chlorella* sp. UMACC 258 and *Synechococcus* sp. UMACC 371. These observations were made over 12-day time frames within the anodic chamber of BPV devices, employing an rGO-CP anode. Data as mean ± S.D., (n = 4).

BPV performances

The effect of the as-synthesized anodes on the performances of the BPV devices was investigated, and the results are shown in Figure 9. Utilizing local tropical marine microalgae, *Chlorella* sp. UMACC 258 and *Synechococcus* sp. UMACC 371, cultivated in Prov medium, as the inoculums in the BPV devices, revealed statistically significant differences in the maximum power density among the different anodes ($F(2,18) = 47.299$, $p < 0.001$). The bare CP anode recorded the lowest power density for both *Chlorella* sp. UMACC 258 and *Synechococcus* sp. UMACC 371, which were 0.02 ± 0.002 mW m^{-2} and 0.063 ± 0.008 mW m^{-2}, respectively (Figure 9A), originated from the restricted electrical conductivity and lower surface area of CP.[35]

Coating of CP with GO prompted a rise in the power density of the BPV device, reaching 0.112 ± 0.01 mW m^{-2} for *Chlorella* sp. UMACC 258 and 0.078 ± 0.012 mW m^{-2} for *Synechococcus* sp. UMACC 371 (Figure 9B). This enhancement could be due to the presence of additional charge carriers on the GO.[35] However, these power density values remained inadequate for commercial use due to the subpar electrical conductivity of GO. Upon removal of the oxygen functional groups of GO, the maximum power density of the BPV device was substantially increased to 0.210 ± 0.04 mW m^{-2} for *Chlorella* sp. UMACC 258 and 0.555 ± 0.09 mW m^{-2} for *Synechococcus* sp. UMACC 371 (Figure 9C). This could be attributed to the improved graphitization of the C=C bond, π–conjugation of the graphene basal plane, and higher number of sp^2 domains as indicated by the increased C/O ratio derived from XPS analysis. As a result, the electrical conductivity of the rGO was greatly enhanced post-reduction.[35,55] Moreover, after the coating of rGO, the pore size and volume of the anode have increased, which leads to better substrate transport and adhesion of microalgae to the anode, thereby improving the EET efficiency from the microalgae to the anode.[29,31] This is supported by the Brunauer-Emmett-Teller (BET) analysis (Figure S1), which showed that rGO has a larger pore size (115.03 Å) and pore volume (0.011478 cm^3/g) compared to GO (21.98 Å and 0.006410 cm^3/g). This could be beneficial for the microalgae attachment, even though GO has a higher BET surface area (11.6636 m^2/g) compared to rGO (3.9912 m^2/g). Similar observation was reported by Ng et al. in which an ITO anode with larger diameter of etched surface resulted in a better growth of cyanobacteria biofilm, *Spirulina* UMACC 159 on the anode, as well as enhanced its photosynthetic performance.[56] In addition, the effect of illumination on the voltage generated by *Synechoccocus* sp. UMACC 371 in rGO-CP BPV was shown in Figure S2. The maximum power density generated by the control setup (Prov medium in rGO-BPV) was only 0.019 ± 0.002 mW m^{-2} (Figure S3). This value is substantially lower compared to rGO-BPV with microalgae culture, indicating that the microalgal cells were the main contributors in bioelectricity generation in the BPV devices.[57]

The maximum power density documented in this research was comparable, if not superior, to BPV studies involving freshwater microalgae. For instance, Ng et al. reported a maximum power density of 0.273 mW m^{-2} and 0.538 mW m^{-2}, generated by *Chlorella* sp. UMACC 313 and

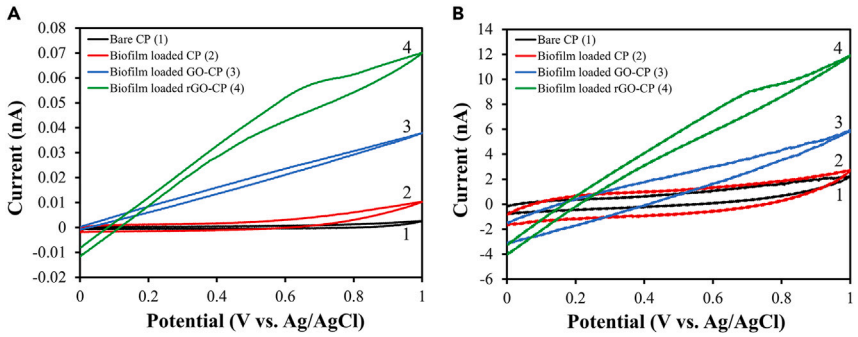

Figure 8. Electrochemical characterization of the as-synthesized anodes

Cyclic voltammograms of the as-synthesized anodes in (A) *Chlorella* sp. UMACC 258 and (B) *Synechococcus* sp. UMACC 371 cultivated in Prov medium at a scan rate of 50 mVs^{-1}.

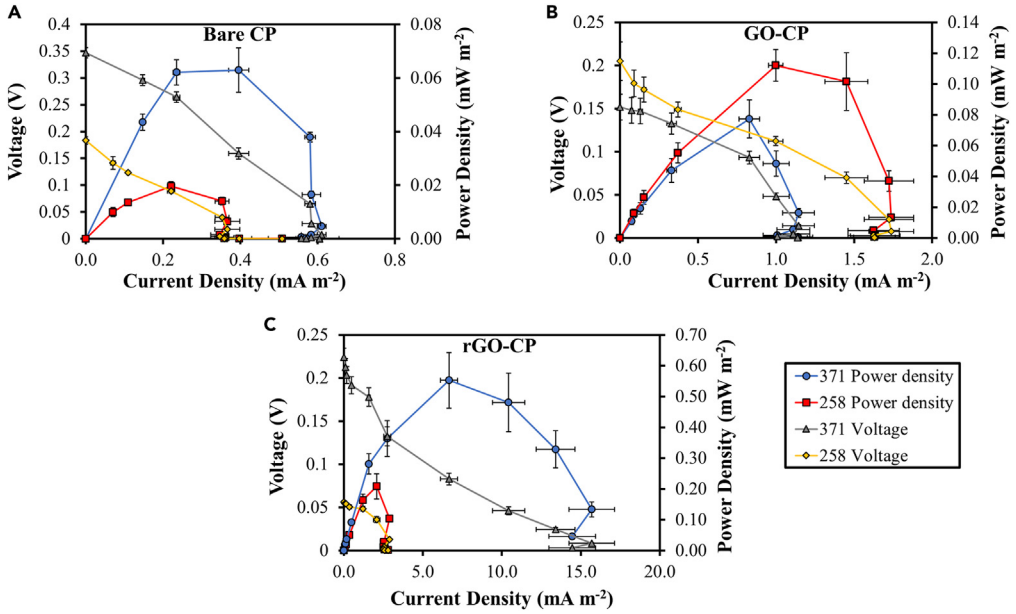

Figure 9. Performances of BPV with different anodes and microalgae strains

Polarization curves of BPV equipped with (A) bare CP, (B) GO-CP, and (C) rGO-CP anode in *Chlorella* sp. UMACC 258 and *Synechococcus* sp. UMACC 371. Data as mean ± S.D., (n = 4).

Synechococcus elongatus UMACC 105, respectively, in BPV device with Langmuir-Blodgett fabricated rGO anode.[31,32] This highlights the potential of employing marine microalgae in the BPV device, as seawater media have elevated electrolyte concentrations compared to freshwater media, resulting in greater conductivity and reduced ohmic losses.[58] Also, this study demonstrated the potential of incorporating microalgal-rGO as a catalyst on the anode of BPV device based on the higher maximum power density generated compared to the other anode materials such as ITO (0.322 mW m^{-2}),[32] ethylene-co-vinyl alcohol-coated PET (0.15 mW m^{-2})[59] and metal organic frameworks (0.04 mW m^{-2}).[17]

Meanwhile, *Synechococcus* sp. UMACC 371 exhibited significantly higher power density than *Chlorella* sp. UMACC 258 across all the tested anodes, except GO-CP. This disparity could be due to the more intricate electrons transportation pathway *Chlorella* sp. UMACC 258, where electrons need to navigate through three obstructive layers: the cell wall, cytoplasmic membrane, and chloroplast membrane due to the presence of chloroplast in eukaryotic algae.[10,60] This complexity hinders the electron transfer process. On the other hand, in prokaryotic cyanobacteria, the photolysis process takes place in the thylakoid membrane, which is directly exposed to the cytoplasm. This configuration requires electrons to pass through fewer obstructive layers in cyanobacteria, resulting in a more streamlined electron transport process. Consequently, this streamlined process leads to the generation of higher power density.[61] Similarly, Ng et al. reported a higher power output from *Synechococcus elongatus* compared to *Chlorella* sp. This difference was attributed to the simpler cellular structure of *Synechococcus elongatus*, which enhanced the EET efficiency.[32] In more complex systems, energy loss occurs with each electron transfer between carrier molecules, making the process less efficient.[61]

Conclusion

Overall, the removal of oxygen functional group from GO was successfully accomplished upon the addition of concentrated *Chlorella* sp. UMACC 313 suspensions. Utilizing rGO-CP as the anode resulted in a notable increase in the maximum power density produced by the BPV device. More precisely, there was a significance enhancement of 950% for *Chlorella* sp. UMACC 258 and 781% for *Synechococcus* sp. UMACC 371, respectively, in comparison to the uncoated CP anode. This improvement can be credited to the expanded specific surface area of rGO, which promotes improved adhesion of microalgae to the anode, as confirmed by SEM observations. Consequently, this enhancement boosts the EET efficiency from microalgae to the anode. Eliminating the oxygen functional groups led to a notable enhancement in the electrical conductivity of rGO, primarily due to the reestablishment of π-conjugation in graphene. This reinstated π-conjugation played a pivotal role in augmenting the observed power density in the present investigation. This research highlights the potential of utilizing indigenous tropical marine microalgae in BPV devices, with specific focus on *Synechococcus* sp. UMACC 371, which exhibited a greater power density in comparison to *Chlorella* sp. UMACC 258.

Limitations of the study

The reduction of GO by microalgae offers the prospect of making BPV production more cost-effective, thereby lowering the costs linked to widespread implementation on a larger scale. Nonetheless, it is essential to delve into the mechanisms that govern the reduction of GO by

microalgae and identifying the molecules responsible for eliminating oxygen functional groups. This endeavor is crucial to further improve the reduction process and advance the goal of environmentally friendly large-scale synthesis of rGO.

STAR★METHODS

Detailed methods are provided in the online version of this paper and include the following:

- KEY RESOURCES TABLE
- RESOURCE AVAILABILITY
  - Lead contact
  - Materials availability
  - Data and code availability
- EXPERIMENTAL MODEL AND STUDY PARTICIPANT DETAILS
- METHOD DETAILS
  - Preparation of microalgal suspension
  - Reduction of graphene oxide by using microalgal suspension
  - Modification of anodes
  - Characterization of materials
  - Marine microalgae culture
  - Growth performance of microalgae
  - Photosynthetic efficiency of microalgae
  - Cyclic voltammetry (CV) measurements
  - BPV devices set up and measurements
- QUANTIFICATION AND STATISTICAL ANALYSIS
- ADDITIONAL RESOURCES

SUPPLEMENTAL INFORMATION

Supplemental information can be found online at https://doi.org/10.1016/j.isci.2024.109564.

ACKNOWLEDGMENTS

This work was supported by the Ministry of Higher Education Malaysia via Fundamental Research Grant Scheme (FRGS) (FRGS/1/2022/TK08/UM/03/1)(FP098-2022) and Hainan Provincial Natural Science Foundation of China (521CXTD439).

AUTHOR CONTRIBUTIONS

Conceptualization, S.M.P., G.G.K., and F.L.N.; methodology, J.Y.T., F.L.N., and F.K.S.L.; investigation, J.Y.T.; resources, B.Z. and S.L.; writing – original draft, J.Y.T.; writing – review and editing, F.L.N., F.K.S.L., B.Z., and G.G.K.; supervision, S.M.P., G.G.K., and F.L.N.; funding acquisition, S.M.P., F.K.S.L., and S.L.

DECLARATION OF INTERESTS

The authors declare no competing interests.

Received: October 19, 2023
Revised: February 28, 2024
Accepted: March 22, 2024
Published: March 26, 2024

REFERENCES

1. Lewis, N.S., and Nocera, D.G. (2006). Powering the planet: Chemical challenges in solar energy utilization. Proc. Natl. Acad. Sci. USA *103*, 15729–15735. https://doi.org/10.1073/pnas.0603395103.
2. Khan, M.I., Shin, J.H., and Kim, J.D. (2018). The promising future of microalgae: current status, challenges, and optimization of a sustainable and renewable industry for biofuels, feed, and other products. Microb. Cell Fact. *17*, 36. https://doi.org/10.1186/s12934-018-0879-x.
3. Goswami, R.K., Mehariya, S., Obulisamy, P.K., and Verma, P. (2021). Advanced microalgae-based renewable biohydrogen production systems: A review. Bioresour. Technol. *320*, 124301. https://doi.org/10.1016/j.biortech.2020.124301.
4. Jacob, A., Ashok, B., Alagumalai, A., Chyuan, O.H., and Le, P.T.K. (2021). Critical review on third generation micro algae biodiesel production and its feasibility as future bioenergy for IC engine applications. Energy Convers. Manag. *228*, 113655. https://doi.org/10.1016/j.enconman.2020.113655.
5. Phwan, C.K., Ong, H.C., Chen, W.-H., Ling, T.C., Ng, E.P., and Show, P.L. (2018). Overview: Comparison of pretreatment technologies and fermentation processes of bioethanol from microalgae. Energy Convers. Manag. *173*, 81–94. https://doi.org/10.1016/j.enconman.2018.07.054.
6. Ng, F.L., Phang, S.M., Thong, C.H., Periasamy, V., Pindah, J., Yunus, K., and Fisher, A.C. (2021). Integration of

bioelectricity generation from algal biophotovoltaic (BPV) devices with remediation of palm oil mill effluent (POME) as substrate for algal growth. Environ. Technol. Innov. *21*, 101280. https://doi.org/10.1016/j.eti.2020.101280.

7. Thong, C.H., Ng, F.L., Periasamy, V., Basirun, W.J., Kumar, G.G., and Phang, S.M. (2023). Sustained power output from an algal biophotovoltaic (BPV) platform using selected marine and freshwater microalgae. J. Appl. Phycol. *35*, 131–143. https://doi.org/10.1007/s10811-022-02879-9.
8. Periasamy, V., Jaafar, M.M., Chandrasekaran, K., Talebi, S., Ng, F.L., Phang, S.M., kumar, G.G., and Iwamoto, M. (2022). Langmuir-Blodgett graphene-based films for algal biophotovoltaic fuel cells. Nanomaterials *12*, 840. https://doi.org/10.3390/nano12050840.
9. Chen, X., Lawrence, J.M., Wey, L.T., Schertel, L., Jing, Q., Vignolini, S., Howe, C.J., Kar-Narayan, S., and Zhang, J.Z. (2022). 3D-printed hierarchical pillar array electrodes for high-performance semi-artificial photosynthesis. Nat. Mater. *21*, 811–818. https://doi.org/10.1038/s41563-022-01205-5.
10. Zhu, H., Wang, H., Zhang, Y., and Li, Y. (2023). Biophotovoltaics: Recent advances and perspectives. Biotechnol. Adv. *64*, 108101. https://doi.org/10.1016/j.biotechadv.2023.108101.
11. Schneider, K., Thorne, R.J., and Cameron, P.J. (2016). An investigation of anode and cathode materials in photomicrobial fuel cells. Philos. Trans. Royal Soc. A *374*, 20150080. https://doi.org/10.1098/rsta.2015.0080.
12. Ng, F.L., Phang, S.M., Periasamy, V., Yunus, K., and Fisher, A.C. (2014). Evaluation of algal biofilms on indium tin oxide (ITO) for use in biophotovoltaic platforms based on photosynthetic performance. PLoS One *9*, e97643. https://doi.org/10.1371/journal.pone.0097643.
13. Thorne, R., Hu, H., Schneider, K., Bombelli, P., Fisher, A., Peter, L.M., Dent, A., and Cameron, P.J. (2011). Porous ceramic anode materials for photo-microbial fuel cells. J. Mater. Chem. *21*, 18055–18060. https://doi.org/10.1039/C1JM13058G.
14. Sekar, N., Umasankar, Y., and Ramasamy, R.P. (2014). Photocurrent generation by immobilized cyanobacteria via direct electron transport in photo-bioelectrochemical cells. Phys. Chem. Chem. Phys. *16*, 7862–7871. https://doi.org/10.1039/C4CP004A.
15. Zou, Y., Pisciotta, J., and Baskakov, I.V. (2010). Nanostructured polypyrrole-coated anode for sun-powered microbial fuel cells. Bioelectrochemistry *79*, 50–56. https://doi.org/10.1016/j.bioelechem.2009.11.001.
16. Karthikeyan, C., Jenita Rani, G., Ng, F.L., Periasamy, V., Pappathi, M., Jothi Rajan, M., Al-Sehemi, A.G., Pannipara, M., Phang, S.M., Abdul Aziz, M., and Gnana kumar, G. (2020). 3D flower–like $FeWO_4/CeO_2$ hierarchical architectures on rGO for durable and high-performance microalgae biophotovoltaic fuel cells. Appl. Biochem. Biotechnol. *192*, 751–769. https://doi.org/10.1007/s12010-020-03352-4.
17. Thong, C.H., Priyanga, N., Ng, F.L., Pappathi, M., Periasamy, V., Phang, S.M., and Gnana kumar, G. (2022). Metal organic frameworks (MOFs) as potential anode materials for improving power generation from algal biophotovoltaic (BPV) platforms. Catal. Today *397–399*, 419–427. https://doi.org/10.1016/j.cattod.2021.07.020.
18. Choi, W., Lahiri, I., Seelaboyina, R., and Kang, Y.S. (2010). Synthesis of graphene and its applications: A review. Crit. Rev. Solid State Mater. Sci. *35*, 52–71. https://doi.org/10.1080/10408430903505036.
19. Serrano-Luján, L., Víctor-Román, S., Toledo, C., Sanahuja-Parejo, O., Mansour, A.E., Abad, J., Amassian, A., Benito, A.M., Maser, W.K., and Urbina, A. (2019). Environmental impact of the production of graphene oxide and reduced graphene oxide. SN Appl. Sci. *1*, 179. https://doi.org/10.1007/s42452-019-0193-1.
20. Agarwal, V., and Zetterlund, P.B. (2021). Strategies for reduction of graphene oxide – A comprehensive review. Chem. Eng. J. *405*, 127018. https://doi.org/10.1016/j.cej.2020.127018.
21. Fernández-Merino, M.J., Guardia, L., Paredes, J.I., Villar-Rodil, S., Solís-Fernández, P., Martínez-Alonso, A., and Tascón, J.M.D. (2010). Vitamin C is an ideal substitute for hydrazine in the reduction of graphene oxide suspensions. J. Phys. Chem. C *114*, 6426–6432. https://doi.org/10.1021/jp100603h.
22. Khan, M., Al-Marri, A.H., Khan, M., Shaik, M.R., Mohri, N., Adil, S.F., Kuniyil, M., Alkhathlan, H.Z., Al-Warthan, A., Tremel, W., et al. (2015). Green approach for the effective reduction of graphene oxide using *Salvadora persica* L. root (Miswak) extract. Nanoscale Res. Lett. *10*, 987. https://doi.org/10.1186/s11671-015-0987-z.
23. Salas, E.C., Sun, Z., Lüttge, A., and Tour, J.M. (2010). Reduction of graphene oxide via bacterial respiration. ACS Nano *4*, 4852–4856. https://doi.org/10.1021/nn101081t.
24. Khanna, P., Kaur, A., and Goyal, D. (2019). Algae-based metallic nanoparticles: Synthesis, characterization and applications. J. Microbiol. Methods *163*, 105656. https://doi.org/10.1016/j.mimet.2019.105656.
25. Siddiqi, K.S., and Husen, A. (2016). Fabrication of metal and metal oxide nanoparticles by algae and their toxic effects. Nanoscale Res. Lett. *11*, 363. https://doi.org/10.1186/s11671-016-1580-9.
26. Xie, J., Lee, J.Y., Wang, D.I.C., and Ting, Y.P. (2007a). Identification of active biomolecules in the high-yield synthesis of single-crystalline gold nanoplates in algal solutions. Small *3*, 672–682. https://doi.org/10.1002/smll.200600612.
27. Xie, J., Lee, J.Y., Wang, D.I.C., and Ting, Y.P. (2007b). Silver nanoplates: From biological to biomimetic synthesis. ACS Nano *1*, 429–439. https://doi.org/10.1021/nn7000883.
28. Chia, S.R., Ong, H.C., Chew, K.W., Show, P.L., Phang, S.M., Ling, T.C., Nagarajan, D., Lee, D.J., and Chang, J.S. (2018). Sustainable approaches for algae utilisation in bioenergy production. Renew. Energy *129*, 838–852. https://doi.org/10.1016/j.renene.2017.04.001.
29. Tee, J.Y., Ng, F.L., Keng, F.S.L., Gnana kumar, G., and Phang, S.M. (2023). Microbial reduction of graphene oxide and its application in microbial fuel cells and biophotovoltaics. Front. Mater. Sci. *17*, 230642. https://doi.org/10.1007/s11706-023-0642-z.
30. Zhang, Y., Mo, G., Li, X., Zhang, W., Zhang, J., Ye, J., Huang, X., and Yu, C. (2011). A graphene modified anode to improve the performance of microbial fuel cells. J. Power Sources *196*, 5402–5407. https://doi.org/10.1016/j.jpowsour.2011.02.067.
31. Ng, F.L., Jaafar, M.M., Phang, S.M., Chan, Z., Salleh, N.A., Azmi, S.Z., Yunus, K., Fisher, A.C., and Periasamy, V. (2014). Reduced graphene oxide anodes for potential application in algae biophotovoltaic platforms. Sci. Rep. *4*, 7562. https://doi.org/10.1038/srep07562.
32. Ng, F.L., Phang, S.M., Periasamy, V., Beardall, J., Yunus, K., and Fisher, A.C. (2018). Algal biophotovoltaic (BPV) device for generation of bioelectricity using *Synechococcus elongatus* (Cyanophyta). J. Appl. Phycol. *30*, 2981–2988. https://doi.org/10.1007/s10811-018-1515-1.
33. Zhou, Y., Bao, Q., Tang, L.A.L., Zhong, Y., and Loh, K.P. (2009). Hydrothermal dehydration for the "green" reduction of exfoliated graphene oxide to graphene and demonstration of tunable optical limiting properties. Chem. Mater. *21*, 2950–2956. https://doi.org/10.1021/cm9006603.
34. Stankovich, S., Dikin, D.A., Piner, R.D., Kohlhaas, K.A., Kleinhammes, A., Jia, Y., Wu, Y., Nguyen, S.T., and Ruoff, R.S. (2007). Synthesis of graphene-based nanosheets via chemical reduction of exfoliated graphite oxide. Carbon *45*, 1558–1565. https://doi.org/10.1016/j.carbon.2007.02.034.
35. Gnana kumar, G., Kirubaharan, C.J., Udhayakumar, S., Ramachandran, K., Karthikeyan, C., Renganathan, R., and Nahm, K.S. (2014). Synthesis, structural, and morphological characterizations of reduced graphene oxide-supported polypyrrole anode catalysts for improved microbial fuel cell performances. ACS Sustain. Chem. Eng. *2*, 2283–2290. https://doi.org/10.1021/sc500244f.
36. Gurunathan, S., Han, J.W., Eppakayala, V., and Kim, J.H. (2013). Microbial reduction of graphene oxide by Escherichia coli: A green chemistry approach. Colloids Surf., B *102*, 772–777. https://doi.org/10.1016/j.colsurfb.2012.09.011.
37. Li, D., Müller, M.B., Gilje, S., Kaner, R.B., and Wallace, G.G. (2008). Processable aqueous dispersions of graphene nanosheets. Nat. Nanotechnol. *3*, 101–105. https://doi.org/10.1038/nnano.2007.451.
38. Sharma, N., Sharma, V., Jain, Y., Kumari, M., Gupta, R., Sharma, S.K., and Sachdev, K. (2017). Synthesis and characterization of graphene oxide (GO) and reduced graphene oxide (rGO) for gas sensing application. Macromol. Symp. *376*, 1700006. https://doi.org/10.1002/masy.201700006.
39. Park, S., An, J., Jung, I., Piner, R.D., An, S.J., Li, X., Velamakanni, A., and Ruoff, R.S. (2009). Colloidal suspensions of highly reduced graphene oxide in a wide variety of organic solvents. Nano Lett. *9*, 1593–1597. https://doi.org/10.1021/nl803798y.
40. Saleem, H., Haneef, M., and Abbasi, H.Y. (2018). Synthesis route of reduced graphene oxide via thermal reduction of chemically exfoliated graphene oxide. Mater. Chem. Phys. *204*, 1–7. https://doi.org/10.1016/j.matchemphys.2017.10.020.
41. Andrijanto, E., Shoelarta, S., Subiyanto, G., and Rifki, S. (2016). Facile synthesis of graphene from graphite using ascorbic acid as reducing agent. AIP Conf. Proc. *1725*, 020003. https://doi.org/10.1063/1.4945457.
42. Li, Z., Deng, L., Kinloch, I.A., and Young, R.J. (2023). Raman spectroscopy of carbon materials and their composites: Graphene, nanotubes and fibres. Prog. Mater. Sci. *135*, 101089. https://doi.org/10.1016/j.pmatsci.2023.101089.
43. Liao, J., Zhang, X., Sun, Z., Chen, H., Fu, J., Si, H., Ge, C., and Lin, S. (2022). Laser-induced

graphene-based wearable epidermal ion-selective sensors for noninvasive multiplexed sweat analysis. Biosensors *12*, 397. https://doi.org/10.3390/bios12060397.

44. Al-Gaashani, R., Najjar, A., Zakaria, Y., Mansour, S., and Atieh, M.A. (2019). XPS and structural studies of high quality graphene oxide and reduced graphene oxide prepared by different chemical oxidation methods. Ceram. Int. *45*, 14439–14448. https://doi.org/10.1016/j.ceramint.2019.04.165.
45. Hu, J., Kong, G., Zhu, Y., and Che, C. (2021). Ultrafast room-temperature reduction of graphene oxide by sodium borohydride, sodium molybdate and hydrochloric acid. Chin. Chem. Lett. *32*, 543–547. https://doi.org/10.1016/j.cclet.2020.03.045.
46. Shin, H.-J., Kim, K.K., Benayad, A., Yoon, S.-M., Park, H.K., Jung, I.-S., Jin, M.H., Jeong, H.-K., Kim, J.M., Choi, J.-Y., and Lee, Y.H. (2009). Efficient reduction of graphite oxide by sodium borohydride and its effect on electrical conductance. Adv. Funct. Mater. *19*, 1987–1992. https://doi.org/10.1002/adfm.200900167.
47. Nandgaonkar, A.G., Wang, Q., Fu, K., Krause, W.E., Wei, Q., Gorga, R., and Lucia, L.A. (2014). A one-pot biosynthesis of reduced graphene oxide (RGO)/bacterial cellulose (BC) nanocomposites. Green Chem. *16*, 3195–3201. https://doi.org/10.1039/C4GC00264D.
48. Wang, G., Qian, F., Saltikov, C.W., Jiao, Y., and Li, Y. (2011). Microbial reduction of graphene oxide by *Shewanella*. Nano Res. *4*, 563–570. https://doi.org/10.1007/s12274-011-0112-2.
49. Yang, Z.Z., Zheng, Q.B., Qiu, H.X., Li, J., and Yang, J.H. (2015). A simple method for the reduction of graphene oxide by sodium borohydride with $CaCl_2$ as a catalyst. New Carbon Mater. *30*, 41–47. https://doi.org/10.1016/S1872-5805(15)60174-3.
50. Zhang, Y., He, Q., Xia, L., Li, Y., and Song, S. (2018). Algae cathode microbial fuel cells for cadmium removal with simultaneous electricity production using nickel foam/graphene electrode. Biochem. Eng. J. *138*, 179–187. https://doi.org/10.1016/j.bej.2018.07.021.
51. Si, Y., and Samulski, E.T. (2008). Synthesis of water soluble graphene. Nano Lett. *8*, 1679–1682. https://doi.org/10.1021/nl080604h.
52. Hou, D., Liu, Q., Cheng, H., Zhang, H., and Wang, S. (2017). Green reduction of graphene oxide via *Lycium barbarum* extract. J. Solid State Chem. *246*, 351–356. https://doi.org/10.1016/j.jssc.2016.12.008.
53. Muthoosamy, K., Bai, R.G., Abubakar, I.B., Sudheer, S.M., Lim, H.N., Loh, H.S., Huang, N.M., Chia, C.H., and Manickam, S. (2015). Exceedingly biocompatible and thin-layered reduced graphene oxide nanosheets using an eco-friendly mushroom extract strategy. Int. J. Nanomed. *10*, 1505–1519. https://doi.org/10.2147/IJN.S75213.
54. Reeves, S., McMinn, A., and Martin, A. (2011). The effect of prolonged darkness on the growth, recovery and survival of Antarctic sea ice diatoms. Polar Biol. *34*, 1019–1032. https://doi.org/10.1007/s00300-011-0961-x.
55. Zhu, W., Gao, H., li, P., Li, Y., Zhang, J., and Bai, H. (2021). The interaction between microbes and electrodes decorated with bio-reduced graphene oxide— from an electrochemical point of view. J. Chem. Technol. Biotechnol. *96*, 172–179. https://doi.org/10.1002/jctb.6524.
56. Ng, F.L., Phang, S.M., Periasamy, V., Yunus, K., and Fisher, A.C. (2014). Algae biofilm on indium tin oxide electrode for use in biophotovoltaic platforms. Adv. Mat. Res. *895*, 116–121. https://doi.org/10.4028/www.scientific.net/AMR.895.116.
57. Thong, C.H., Phang, S.M., Ng, F.L., Periasamy, V., Ling, T.C., Yunus, K., and Fisher, A.C. (2019). Effect of different irradiance levels on bioelectricity generation from algal biophotovoltaic (BPV) devices. Energy Sci. Eng. *7*, 2086–2097. https://doi.org/10.1002/ese3.414.
58. McCormick, A.J., Bombelli, P., Scott, A.M., Philips, A.J., Smith, A.G., Fisher, A.C., and Howe, C.J. (2011). Photosynthetic biofilms in pure culture harness solar energy in a mediatorless bio-photovoltaic cell (BPV) system. Energy Environ. Sci. *4*, 4699–4709. https://doi.org/10.1039/C1EE01965A.
59. Chen, W.-J., Lee, M.-H., Thomas, J.L., Lu, P.-H., Li, M.-H., and Lin, H.-Y. (2013). Microcontact Imprinting of Algae on Poly(ethylene-co-vinyl alcohol) for Biofuel Cells. ACS Appl. Mater. Interfaces *5*, 11123–11128. https://doi.org/10.1021/am403313p.
60. Wey, L.T., Bombelli, P., Chen, X., Lawrence, J.M., Rabideau, C.M., Rowden, S.J.L., Zhang, J.Z., and Howe, C.J. (2019). The development of biophotovoltaic systems for power generation and biological analysis. Chemelectrochem *6*, 5375–5386. https://doi.org/10.1002/celc.201900997.
61. Bradley, R.W., Bombelli, P., Rowden, S.J.L., and Howe, C.J. (2012). Biological photovoltaics: Intra- and extra-cellular electron transport by cyanobacteria. Biochem. Soc. Trans. *40*, 1302–1307. https://doi.org/10.1042/BST20120118.
62. Phang, S., and Chu, W. (1999). University of Malaya Algae Culture Collection (UMACC), 77 (Catalogue of Strain. Institute of Postgraduate Studies and Research, University of Malaya).
63. Nichols, H.W., and Bold, H.C. (1965). *Trichosarcina polymorpha* Gen. et Sp. Nov. J. Phycol. *1*, 34–38. https://doi.org/10.1111/j.1529-8817.1965.tb04552.x.
64. Ji, X., Song, Y., Han, J., Ge, L., Zhao, X., Xu, C., Wang, Y., Wu, D., and Qiu, H. (2017). Preparation of a stable aqueous suspension of reduced graphene oxide by a green method for applications in biomaterials. J. Colloid Interface Sci. *497*, 317–324. https://doi.org/10.1016/j.jcis.2016.09.049.
65. Ahmad, S., Ahmad, A., Khan, S., Ahmad, S., Khan, I., Zada, S., and Fu, P. (2019). Algal extracts based biogenic synthesis of reduced graphene oxides (rGO) with enhanced heavy metals adsorption capability. J. Ind. Eng. Chem. *72*, 117–124. https://doi.org/10.1016/j.jiec.2018.12.009.
66. Tay, Z.H.Y., Ng, F.L., Thong, C.H., Lee, C.W., Gnana kumar, G., Al-Sehemi, A.G., and Phang, S. M. (2024). Evaluation of selected tropical marine microalgal cultures for use in biophotovoltaic platforms. Appl. Microbiol. Biotechnol. *108*, 71. https://doi.org/10.1007/s00253-023-12951-0.
67. Lim, Y.K., Phang, S.M., Sturges, W.T., Malin, G., and Rahman, N.B.A. (2018). Emission of short-lived halocarbons by three common tropical marine microalgae during batch culture. J. Appl. Phycol. *30*, 341–353. https://doi.org/10.1007/s10811-017-1250-z.
68. Strickland, J.D.H., and Parsons, T.R. (1972). A Practical Handbook of Seawater Analysis, Second ed. (Fisheries Research Board of Canada).
69. Karsten, U., Koch, S., West, J.A., and Kirst, G.O. (1996). Physiological responses of the eulittoral macroalga *Stictosiphonia hookeri* (Rhodomelaceae, Rhodophyta) from Argentina and Chile: salinity, light and temperature acclimation. Eur. J. Phycol. *31*, 361–368. https://doi.org/10.1080/09670269600651591.
70. Keng, F.S.L., Phang, S.M., Abd Rahman, N., Yeong, H.Y., Malin, G., Leedham Elvidge, E., and Sturges, W. (2021). Halocarbon emissions by selected tropical seaweeds exposed to different temperatures. Phytochemistry *190*, 112869. https://doi.org/10.1016/j.phytochem.2021.112869.
71. Schreiber, U., Endo, T., Mi, H., and Asada, K. (1995). Quenching analysis of chlorophyll fluorescence by the saturation pulse method: Particular aspects relating to the study of eukaryotic algae and cyanobacteria. Plant Cell Physiol. *36*, 873–882. https://doi.org/10.1093/oxfordjournals.pcp.a078833.

STAR★METHODS

KEY RESOURCES TABLE

REAGENT or RESOURCE	SOURCE	IDENTIFIER
Biological samples		
Chlorella sp.	UMACC	313
Chlorella sp.	UMACC	258
Synechococcus sp.	UMACC	371
Chemicals, peptides, and recombinant proteins		
Nafion™ 117 containing solution	Sigma-Aldrich	31175-20-9
Graphene oxide	Abalonxy, currently known as LayerOne	NA
Toray Carbon Paper, PTFE treated, TGP-H-060	Alfa Aesar, Thermo Scientific	7782-42-5
Nafion 115	Fuel Cell Store	591439
0.5 mg/cm^2 10%wt % Pt on Carbon Paper, NRE 212	Fuel Cell Earth	NA

RESOURCE AVAILABILITY

Lead contact

Further information and requests for resources and reagents should be directed to and will be fulfilled by the lead contact, phang@um.edu.my (Siew-Moi Phang).

Materials availability

There are restrictions to the availability of the microalgal-reduced graphene oxide due to patent of this material is in progress.

Data and code availability

- The data reported in this paper will be shared by the lead contact upon request.
- This paper does not report original code.
- Any additional information required to reanalyze the data reported in this paper is available from the lead contact upon request.

EXPERIMENTAL MODEL AND STUDY PARTICIPANT DETAILS

There are no experimental model and study participant details to be reported.

METHOD DETAILS

Preparation of microalgal suspension

Chlorella sp. UMACC 313 from the University of Malaya Algae Culture Collection (UMACC)[62] was selected for the reduction of GO due to its higher biochemical composition and growth rate.[12] An inoculum size of 20% from the cultures in the exponential phase, standardized at an optical density of 0.2 at 620 nm ($OD_{620\ nm}$ = 0.2), was introduced into 250 mL conical flasks containing 150 mL of Bold's Basal Medium (BBM).[63] The flasks were placed on an incubator shaker (120 rpm) at 25°C, with an irradiance of 40 μmol photons m^{-2} s^{-1}, following a 12-h light:12-h dark cycle.

After 14 days, the microalgal suspension was prepared by harvesting the microalgal biomass via a centrifugation at 3000 rpm for 10 min. The supernatant was then discarded, and the biomass underwent multiple washes using ultrapure water before being redispersed in ultrapure water to ensure the complete removal of BBM medium that might contribute to the reduction of GO. The optical density of the microalgal suspension was standardized to 2.0 at $OD_{620\ nm}$.

Reduction of graphene oxide by using microalgal suspension

A GO dispersion (0.5 mg mL^{-1}) was prepared by adding GO powder (50–100 mesh, Abalonxy, currently known as LayerOne, Norway) into ultrapure water, which was then ultrasonicated for 30 min at room temperature. Different volumes of *Chlorella* sp. UMACC 313 suspensions were subsequently added, and the mixture was placed in a 90°C water bath. The resultant material was obtained by subjecting it to centrifugation at 10000 rpm for 10 min, followed by several washes with ultrapure water and ethanol and dried at 50°C. Similarly, a GO dispersion

without microalgal suspension were kept at the same conditions as control setup. The extent of reduction of GO was monitored through UV-vis spectrophotometer every 24 h (UV-1800, Shimadzu).[64,65]

Modification of anodes

The dispersion of GO/rGO (30 mg mL^{-1}) in Nafion 117 containing solution (Sigma-Aldrich) was loaded to a carbon paper with an area of 2.01 cm^{-2} and dried overnight at 50°C, keeping a constant catalyst loading of 2.5 mg cm^{-2}[17]

Characterization of materials

The surface chemical composition of both GO and rGO was investigated by using various techniques, including Raman spectroscopy (inVia confocal Raman microscope, Renishaw), XRD (SmartLab, Rigaku), FT-IR (Spectrum 400, PerkinElmer) and XPS (Nexsa G2, Thermo Fisher Scientific). The surface morphologies of GO and rGO were examined through SEM (Verios G4, Thermo Fisher Scientific), TEM (Talos F200X G2, Thermo Fisher Scientific) and BET surface area analyzer (ASAP 2020, Micromeritics),.

Marine microalgae culture

Two local tropical marine microalgae strains including chlorophyte *Chlorella* sp. UMACC 258 and the cyanophyte *Synechococcus* sp. UMACC 371 were selected for BPV studies due to their higher power output generation, as observed in a previous study.[66] *Chlorella* sp. UMACC 258 were isolated from a sea bass pond in Sepang, Malaysia, while *Synechococcus* sp. UMACC 371 were isolated from shrimp ponds connected to the Straits of Malacca in Kuala Selangor, Malaysia.[67] The cultures were grown in Prov medium[62] for 5 days.

Growth performance of microalgae

The chlorophyll *a* (chl-*a*) content of the microalgae was determined using a UV-vis spectrophotometer to estimate both the specific growth rate and biomass of the microalgae. Microalgal cells were harvested through Millipore filtration using glass-fiber filter papers (Whatman GF/C, 0.45 μm). These filter papers were then transferred into the centrifuge tubes and mashed into small pieces in 10 mL of analytical-grade 100% acetone. After being stored overnight at 4°C in the dark, the extracts were subjected to centrifugation at 3000 rpm for 10 min, and the absorbance of the supernatants were read at wavelengths of 630, 645 and 665 nm. The chl-*a* content of the microalgal culture was calculated as follows:[68]

$$\text{chl} - a\ (\text{mg L}^{-1}) = \frac{(C_a \times V_a)}{V_c \times 1000}$$

where

$C_a = 11.6 \times OD_{665\ nm} - 1.31 \times OD_{645\ nm} - 0.14 \times OD_{630\ nm}$

V_a = Volume of acetone (mL) used for extraction.

V_c = Volume of microalgal culture (L)

The specific growth rate, μ (d^{-1}) of the microalgae was calculated based on chl-*a* content as follows:[69]

$$\mu, d^{-1} = \frac{ln(N_2/N_1)}{(t_2 - t_1)}$$

where

N_2 = chl-*a* (mg L^{-1}) at t_2

N_1 = chl-*a* (mg L^{-1}) at t_1

t_2 and t_1 = duration within the exponential phase.

Photosynthetic efficiency of microalgae

The physiological state of the microalgae was evaluated through the maximum quantum yield of the photosystem II (F_v/F_m), measured using the Pulse Amplitude Modulation (PAM) fluorometry method.[70] The microalgae were dark adapted for 15 min prior to the measurement. Then, a weak measuring light from the Diving-PAM fluorometer (Walz, Germany) was applied to determine the minimum fluorescence (F_0), followed by a saturation pulse to determine the maximal fluorescence (F_m). F_v/F_m was subsequently determined using the formula $F_v/F_m = (F_m\text{-}F_0)/F_m$.[71]

Cyclic voltammetry (CV) measurements

A three-electrode setup was established to conduct cyclic voltammetry (CV) tests, which includes a working electrode housing a biofilm or a bare anode, a platinum wire serving as the counter electrode, and an Ag/AgCl electrode functioning as the reference electrode. The above three-electrode setup was immersed in the cultures of *Chlorella* sp. UMACC 258 and *Synechococcus* sp. UMACC 371 grown in Prov medium and CV measurements were conducted using potentiostat (Autolab PGSTAT204, Metrohm) with a scan rate of 50 mV s^{-1}[17]

BPV devices set up and measurements

Bare carbon paper (CP)/GO-loaded CP (GO-CP)/rGO-loaded CP (rGO-CP) and 10% Pt/C-loaded CP (Pt/C/CP) were used, respectively, as anode and cathode. Copper wires were affixed to both the anode and cathode, and they were subsequently linked to the external circuit using alligator clips. The electrodes were divided by a Nafion-115 proton exchange membrane (PEM) (Fuel Cell Store, USA). This membrane was placed inside a perspex chamber and sealed with a polydimethylsiloxane (PDMS) gasket. Afterward, 10 mL of *Chlorella* sp. UMACC 258/*Synechococcus* sp. UMACC 371 (with an optical density at 620nm of 1.0) was introduced onto the anode of each BPV device. The inlet of the BPV devices was sealed using a sterile transparent film roll (Smith & Nephew, UK) to safeguard against any contamination of the cultures.[6] The BPV devices were consistently kept at a temperature of 25°C and exposed to light at an intensity of 90 μmol photons m^{-2} s^{-1} in a 12-h light and 12-h dark cycle for a period of 12 days. On Days 1, 4, 8, and 12, the maximum current and power density of the devices were assessed using an external resistance stepping method. Various external resistances, spanning from 10 MΩ to 1.1 kΩ, were linked to the devices, and the resultant voltages were logged using a data logger (Picolog ADC-24, UK). This data was subsequently employed to create polarization and power curves by applying Ohm's Law.[6] All experiments were performed in quadruplicates, and the displayed results represent the average values.

QUANTIFICATION AND STATISTICAL ANALYSIS

Two-way mixed ANOVA was used to determine if there were differences in the maximum absorption peak (λ_{max}) of rGO at different reaction time and different volume of *Chlorella* sp. UMACC 313 suspensions added. two-way ANOVA was used to test the difference between maximum power density at different anodes and microalgae strains. Statistical analysis was conducted using SPSS Statistics software (IBM, Version 27).

ADDITIONAL RESOURCES

There are no additional resources to be reported.